

Anderson localization effects on doped Hubbard model

Nathan Giovanni,^{1,2} Marcello Civelli,² and Maria C. O. Aguiar^{1,2}

¹*Departamento de Física, Universidade Federal de Minas Gerais,
C.P. 702, 30123-970, Belo Horizonte, MG, Brazil*

²*Université Paris-Saclay, CNRS, Laboratoire de Physique des Solides, 91405, Orsay, France*

(Dated: May 11, 2021)

We derive the disorder vs. doping phase diagram of the doped Hubbard model via Dynamical Mean Field Theory combined with Typical Medium Theory, which allows the description of both Mott (correlation driven) and Anderson (disorder driven) metal-insulator transitions. We observe a transition from a metal to an Anderson-Mott insulator for increasing disorder strength at all interactions. In the weak correlation regime and rather small doping, the Anderson-Mott insulator displays properties which are alike to the ones found at half-filling. In particular, this phase is characterized by the presence of empty sites. If we further increase either the doping or the correlation however, an Anderson-Mott phase of different kind arises for sharply weaker disorder strength. This phase occupies the largest part of the phase diagram in the strong correlation regime, and is characterized by the absence of the empty sites.

I. INTRODUCTION

Mott proposed that electronic correlations can drive a system through a metal-insulator transition (MIT).¹ Hubbard showed that in a half-filled lattice this transition happens when the local correlation contribution is larger than a critical value.² Large correlations are present when a material has a narrow valence band, in which case electrons spread less in the lattice and thus interact more between them, favoring the formation of a Mott insulator.^{3,4} Transition metal oxides are examples of materials where this Mott physics plays a key-role.⁴⁻⁶

In the opposite limit i.e. non-interacting electrons, the presence of disorder can also drive the systems into an insulating phase - the Anderson insulator in this case.^{7,8} Even though there have been improvements in sample growing techniques, effects of disorder are hardly avoidable. Therefore, in doped Mott systems too, disorder plays a non-trivial role, interplaying with doping and correlation. These effects are hard to analyze from both experimental and theoretical perspectives.

In experiments, correlation and disorder effects interplay, for example, in the MIT observed in doped semiconductors, such as Si:P and Si:B,⁹ and in dilute two dimensional electron and hole systems, like silicon metal-oxide-semiconductor field-effect transistors (MOSFET's) and semiconductor heterostructures.^{10,11} More recently, the observation of disorder induced insulator to metal transition has been reported in Mott systems, such as layered dichalcogenide 1T-TaS₂¹² and Ru-substituted Sr₃Ir₂O₇.¹³

From the theoretical viewpoint, the interplay between correlation and disorder can be well described by the Hubbard model solved within extensions of Dynamical Mean Field Theory (DMFT).¹⁴ DMFT description of disorder is equivalent to that of the coherent potential approximation (CPA)¹⁵ and, as such, misses to describe Anderson localization effects.⁷ To circumvent this problem, a mean field treatment of disorder, the so-called Typical Medium Theory (TMT), has been pro-

posed and proved capable of describing the disorder-induced localization.¹⁶⁻¹⁸ The combination of TMT with DMFT has contributed to our understanding of the non-trivial interplay between correlation and disorder localization effects.¹⁹⁻²⁶

In previous works based on DMFT-TMT, an insulating phase which is a mixture of Mott and Anderson insulators has been observed at half-filling.^{20,27} This Anderson-Mott insulator is characterized by the presence of singly-occupied sites, like in a Mott insulator, but has also doubly-occupied and empty sites, like in an Anderson insulator. We shall hereby refer to this Anderson-Mott insulator as AMI-0. Here, we extend these works by investigating the doped-dependent phase diagram of the disordered Hubbard model.

According to our results, in the small correlated regime and moderately low doping, disorder induces an AMI-0 which is alike to the one found in the disorder-driven Anderson-Mott transition at half-filling. As the number of carriers and/or the electronic correlation increases however, the empty sites become occupied and an Anderson-Mott insulator (AMI) different from the AMI-0 observed at half-filling arises. In the strongly correlated regime, the AMI sets in a large part of the disorder versus doping phase diagram at much weaker disorder strengths than the AMI-0. This shows in particular that the doped strongly correlated metal is more susceptible to Anderson-Mott induced localization than the weakly correlated metal.

The paper is organized as follows. In the next section we define the model and describe the methodology used to solve it. Section III is devoted to the presentation and discussion of the disorder versus doping phase diagrams built for different values of the electronic correlation. In subsection III A, we study the AMI-0 region of the phase diagrams, that displays properties similar to the ones of the AMI-0 known at half-filling. In Sec. IV we explore in details the results obtained in the strong correlation regime $U/4t = 3$ and characterize the rising of a different disorder-driven AMI, which has no empty sites. Finally,

Sec. V contains a summary of our conclusions.

II. MODEL AND METHODOLOGY

We focus on the effects of doping the Anderson-Hubbard model (AHM), which is given by the Hamiltonian

$$H = -t \sum_{\langle ij \rangle \sigma} (c_{i\sigma}^\dagger c_{j\sigma} + c_{j\sigma}^\dagger c_{i\sigma}) + U \sum_i n_{i\uparrow} n_{i\downarrow} + \sum_{i\sigma} (\varepsilon_i - \mu) n_{i\sigma}, \quad (1)$$

where $c_{i\sigma}^\dagger$ ($c_{i\sigma}$) creates (destroys) an electron with spin σ on site i , $n_{i\sigma} = c_{i\sigma}^\dagger c_{i\sigma}$, t is the hopping amplitude for nearest neighbor sites, U is the on-site repulsion, ε_i is the random on-site energy, which follows a uniform probability distribution $P(\varepsilon)$ centered in $\varepsilon = 0$ and of width W . μ is the chemical potential, which sets the doping according to $\delta = 2 \langle n_{i\sigma} \rangle_{av} - 1$, with respect to the parent compound ($\delta = 0$) which is nominally at half-filling ($\langle n_{i\sigma} \rangle_{av} = 1/2$; here $\langle \dots \rangle_{av}$ denotes an arithmetic average over disorder of the expectation value of the occupation number operator. We fix here and through the paper the non-interacting bandwidth $4t = 1$ as energy unit. Temperature is set to $T = 0.01$. We consider the paramagnetic solution of the model, observed experimentally, for example, in V_2O_3 at high temperatures.^{28,29}

To be able to describe the correlated Mott transition, we use DMFT.¹⁴ In this methodology, a clean lattice problem is mapped onto an auxiliary single-impurity problem, whose conduction electron bath is determined self-consistently. In the disordered case, the mapping is onto an ensemble of impurity problems, each corresponding to a different value of the parameter that is randomly distributed [on-site energy ε_i in eq. (1)]. DMFT self-consistency involves taking an (arithmetic) average over this ensemble. However, average values do not describe well the asymmetric distributions generated by strong disorder.⁷ As a drawback, DMFT is not able to capture the Anderson transition. By considering the most probable or typical value over the ensemble, instead of the average one, TMT treatment of disorder has been proved capable of describing Anderson localization.^{16,17} Here we use the combination of DMFT and TMT to solve the AHM (eq. 1) and describe the interplay between correlation and disorder induced localization.

Within DMFT-TMT, all the impurities of the ensemble “see” a typical effective medium, which is self-consistently calculated, as follows. We start by considering an initial function $\Delta(\omega)$ that describes this effective medium. By solving the ensemble of single-impurity problems in the presence of this bath, we obtain the self-energies $\Sigma_i(\omega)$ and the local Green’s functions

$$G(\omega, \varepsilon_i) = [\omega + \mu - \varepsilon_i - \Delta(\omega) - \Sigma_i(\omega)]^{-1}, \quad (2)$$

from which local spectra $\rho(\omega, \varepsilon_i) = -\frac{1}{\pi} \text{Im}G(\omega, \varepsilon_i)$ are calculated. In each DMFT-TMT iteration, an effective

medium is calculated: this is given by the *typical or most probable value* of local impurity spectrum, estimated by taking a *geometric average* over the different impurity problems. Precisely, the typical DOS is obtained by the geometric average of $\rho(\omega, \varepsilon)$,

$$\rho_{typ}(\omega) = \exp \left[\int d\varepsilon P(\varepsilon) \ln \rho(\omega, \varepsilon) \right]. \quad (3)$$

The typical Green’s function is then calculated through a Hilbert transform,

$$G_{typ}(\omega) = \int_{-\infty}^{\infty} d\omega' \frac{\rho_{typ}(\omega')}{\omega - \omega'}. \quad (4)$$

As reference case, we consider the Bethe lattice with infinite coordination number, which corresponds to a semi-circular DOS in the non-interacting limit.¹⁴ In this particular case, we close the self-consistent loop by obtaining the new bath function as $\Delta(\omega) = t^2 G_{typ}(\omega)$.

The typical DOS $\rho_{typ}(\omega)$ takes into account only extended states of the system. It is thus critical at the disorder-induced transition, as the system states become localized and $\rho_{typ}(\omega)$ is then expected to go to zero. The (arithmetic) average DOS, which is for instance directly detected in spectroscopic experiments, can also be calculated from the DOS of the single-impurity problems, as follows:

$$\rho_{av}(\omega) = \int d\varepsilon P(\varepsilon) \rho(\omega, \varepsilon). \quad (5)$$

It considers both extended and localized states of the system²⁰ and remains finite at disordered induced MIT. This quantity however goes to zero around the Fermi level by increasing correlation. This signals the correlated-driven Mott MIT.¹⁴

Since the DMFT-TMT self-consistent condition is based on the DOS, it is advantageous to solve the single-impurity problems on the real axis, to avoid an analytic continuation procedure. Here, we solve these auxiliary problems by using perturbation theory in U .^{30,31} Though this method is an approximate solution of the impurity problems which has some well-known drawbacks (e.g. it misses the value of the Kondo temperature), it provides a correct description of the correlated metal to insulator transition, which is the goal of this study. Away from half-filling, the modified second order perturbative contribution in U is given by an expression that interpolates between the known results at high frequencies and at the atomic limit.^{30,31} Comparisons of this approximation with exact diagonalization³¹ and QMC³² results give us confidence in it. Besides directly providing the spectra, this method has the crucial advantage of being numerically fast to allow us to build the phase diagram of disordered problems. For each set of the model parameters, we typically solve hundreds of single-impurity problems in each DMFT-TMT iterative step. The single-impurity code used in this work was developed by Jaksa Vučićević and Darko Tanasković, from the Institute of Physics in

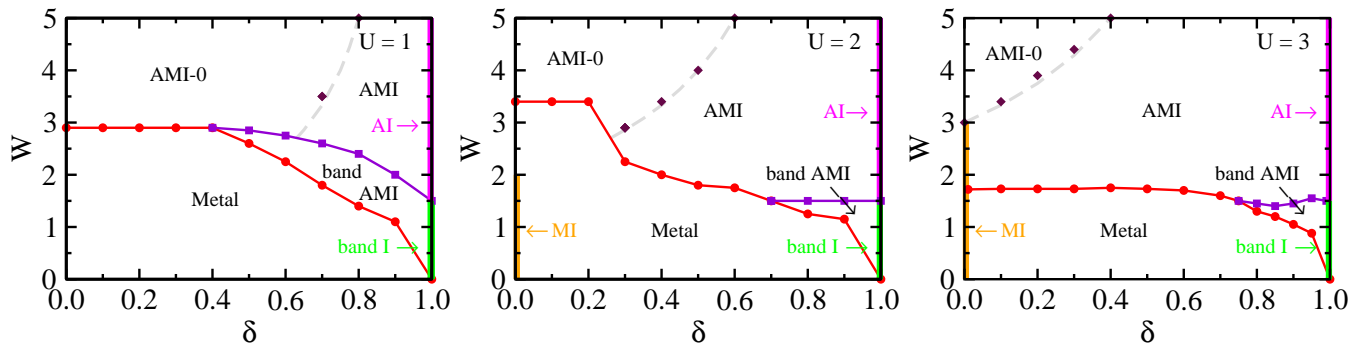


FIG. 1. Disorder (W) versus doping (δ) phase diagram of the doped Anderson-Hubbard model obtained within DMFT-TMT for $U = 1$, $U = 2$, and $U = 3$ at $T = 0.01$. “A” stands for Anderson, “M” for Mott, and “I” for insulator. Inside the Anderson-Mott insulator phase, we have a region where empty sites are present in the system, identified as AMI-0 in the figure, and another region where empty sites are absent, referred to as AMI. A third region inside the Anderson-Mott insulator is that of a band AMI. See text for a complete description of the different phases and regions.

Belgrade, Serbia, and was previously used by one of us in Ref. 22.

When entering into the AMI and AMI-0 regions of the phase diagram, $\rho_{typ}(\omega)$ goes to zero, i.e. $\Delta(\omega) \rightarrow 0$, which means that effectively the Green’s function in eq. (2) reduces to the atomic limit one:³³

$$G_{d\sigma}(\omega) = \frac{1 - \langle n_{i-\sigma} \rangle}{\omega - \varepsilon_d} + \frac{\langle n_{i-\sigma} \rangle}{\omega - \varepsilon_d - U}, \quad (6)$$

where $\varepsilon_d = \varepsilon_i - \mu$ is the impurity local energy (see eq. 1), and $\langle n_{i\sigma} \rangle$ depends on the Fermi-Dirac distribution:

$$\langle n_{i\sigma} \rangle = \frac{1/2}{1 + e^{(\varepsilon_d + U)/T}} + \frac{1/2}{1 + e^{\varepsilon_d/T}}. \quad (7)$$

$\langle n_{i\sigma} \rangle$ can describe singly-occupied sites (typical of a Mott insulator) as well as doubly-occupied and empty sites (typical of an Anderson insulator); these are the occupations that can appear in the AMI and AMI-0 regions, according to the system parameters (U , W , δ), as we mentioned in the Introduction. We shall plug the explicit analytical expressions (6) and (7) into eq. (5) to calculate directly $\rho_{av}(\omega)$ in the AMI and AMI-0 regions. This prevents eventual spurious oscillations that could appear from the discrete finite number of impurities considered, and which can spoil the correct interpretation of $\rho_{av}(\omega)$, especially close to the Fermi level. In the next sections, we shall analyze both quantities $\rho_{typ}(\omega)$ and $\rho_{av}(\omega)$ and characterize the phases appearing in the AHM phase diagram.

III. DISORDER VS. DOPING PHASE DIAGRAMS

In Fig. 1, we present the disorder W vs. doping δ phase diagram of the doped AHM obtained for three different values of correlation: weak correlation $U = 1$, intermediate correlation $U = 2$, and strong correlation $U = 3$.

For rather small disorder ($W < 3$), at half-filling the three cases analyzed in Fig. 1 are different:²² for $U = 1$ the system is in a metallic phase, for $U = 3$ it is in a Mott insulating phase (represented by the orange line at $\delta = 0$ in the phase diagram), and $U = 2$ is an intermediate case, since it is a Mott insulator for small disorder (orange line in Fig. 1) and a metal for intermediate W . It is well known that in the correlated case, upon doping the Mott insulator, states appear at the Fermi level.¹⁴ Thus, for all the three values of U in Fig. 1 we observe a correlated metallic phase for a large range of doping and small disorder.

As disorder increases, a transition to Anderson-Mott insulator takes place in the three cases at a critical disorder W_c . For $U = 1$ and $U = 3$ at *small and intermediate values of doping*, W_c is practically doping independent. We remark that W_c is smaller for $U = 3$ than for $U = 1$, and in particular for the former case W_c is smaller than $W_c \simeq U$, the critical disorder value separating the correlated Mott insulator from the AMI-0 at half-filling (end of the orange line in the phase diagram). If we now look at the results for $U = 2$, the (red) W_c line shows a dependence with doping: it is close to the half-filling value at small doping and, by increasing δ , it decreases towards the same value observed for $U = 3$ (compare W_c for $U = 2$ and $U = 3$ at $\delta \approx 0.7$). W_c vs. δ for $U = 2$ thus interpolates between what is observed for $U = 1$ and $U = 3$.

The comparison between the weak ($U = 1$) and strong ($U = 3$) correlated phase diagrams described above seems then to suggest that the metal that appears upon doping the Mott insulator is more susceptible to disorder induced localization than the metal which sets at small U . At larger U , correlations strongly reduce the quasiparticle bandwidth at the Fermi level (by a factor of Z , the quasiparticle residue), by transferring spectral weight from low to high energies. This forms the well known Mott peak-Hubbard band electronic structure.¹⁴ In this region of the phase diagram, the narrow peak indicates

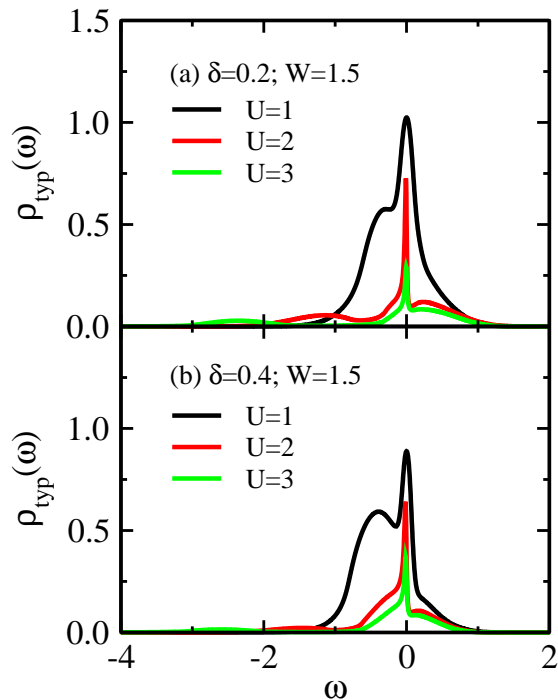


FIG. 2. Comparison of the typical DOS as a function of frequency for $U = 1$, $U = 2$, and $U = 3$ at a disorder value chosen such that the systems are in the metallic phase, $\delta = 0.2$ in panel (a) and $\delta = 0.4$ in panel (b). Although disorder is $W = 1.5$ in all cases, as U increases the system is closer to the MIT.

that quasiparticle are less itinerant, therefore more easily localized by disorder. A critical W_c , smaller than that in the weak correlation region, is sufficient to localize quasiparticles. Indeed, if we compare the typical DOS for the different values of U at $W = 1.5$, shown in Fig. 2, we observe that $\rho_{typ}(\omega)$ decreases as U increases. The transition occurs when $\rho_{typ}(\omega)$ vanishes, since this indicates that extended states of the system fully localize (we will discuss this in more detail in Sec. IV A). This implies that the system with $U = 3$ is closer to Anderson MIT than the one with $U = 1$.

The comparison between $U = 1$ and $U = 3$ results indicate that the metal-Anderson-Mott insulator transition in the weak correlation, where the AMI-0 arises (see next subsection for details), and the transition in the strong correlation regime, where the AMI arises, are sharply different. The AMI in fact is the byproduct of the interplay of disorder with correlation and doping, which suppress empty sites. We shall discuss this in more detail in Sec. IV. For even larger U , the properties of the system are similar to the ones at $U = 3$ when we consider the same doping and disorder values (see Appendix A for details).

Moving now to large doping, for each U value it appears a region that we identify as a *band* AMI. In this case (see section IV A for further details), while electronic states are always present at the Fermi level ($\rho_{av}(\omega = 0) \neq 0$), the typical DOS that describes the extended states

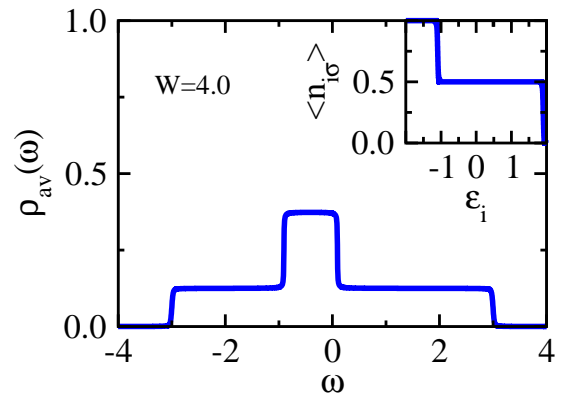


FIG. 3. Average DOS $\rho_{av}(\omega)$ as a function of frequency for $W = 4$ and $\delta = 0.2$, that is, for parameters inside the AMI-0 region of the phase diagram. Inset: occupation number per site and per spin as a function of the on-site energy. $U = 3$ and $T = 0.01$.

shifts to negative frequency and acquires a zero value at the Fermi level, $\rho_{typ}(\omega = 0) = 0$, like the DOS of a band insulator typically does.

By further increasing disorder W , at the strong correlation regime and small doping, the system crossovers from the AMI to the AMI-0, where empty sites are present. This AMI-0 appears at all values of the interaction U (as displayed in Fig. 1), at an Anderson-Mott-like MIT in the small correlation regime ($U = 1$) and as a crossover within the Anderson-Mott insulating phase in the strong correlation regime ($U = 3$). We discuss the properties of this region in detail in the following subsection.

A. The AMI-0 region

We explore in this subsection how the AMI-0 arises within the Anderson-Mott insulating phase, in the large disorder region of the $U = 3$ phase diagram of Fig. 1. This phase is the same kind of insulator that arises at the Anderson-Mott localization at half-filling (see the results for $W = 3.5$ in Appendix B), as we shall show by displaying the spectral function.

In Fig. 3 we show $\rho_{av}(\omega)$ as a function of frequency for $\delta = 0.2$ and $W = 4$, just above the crossover into the AMI-0 region (when coming from smaller values of W , for fixed δ). The average DOS follows the bare distribution of ϵ_i and it is simply given, in the low temperature limit and for $W > U$, by the superposition of two rectangles. In this regime in fact, the DMFT-TMT theory reduces to the superposition of isolated impurities, as we explained in Sec. II [see eqs. (5-7)], and analytical expression can be derived.

The occupation per site and per spin as a function of on-site energy corresponding to the DOS in Fig. 3 is shown in inset. Note that empty sites start to appear, besides those which are doubly- and singly-occupied. We have analyzed other values of δ for $U = 3$, as well as

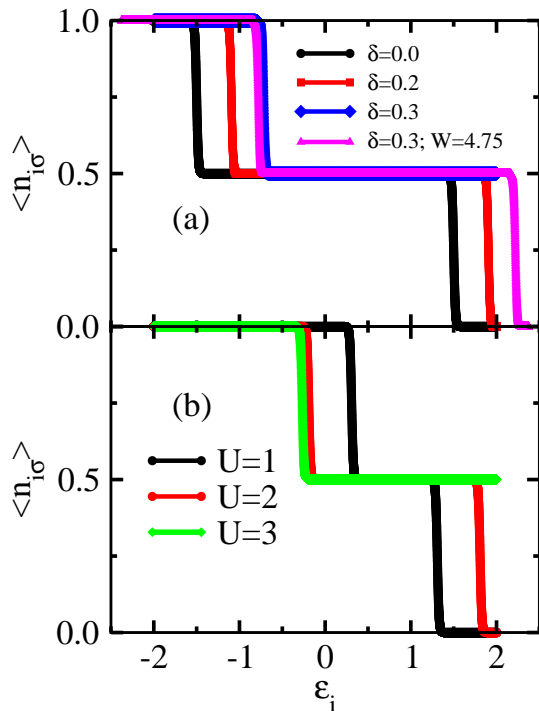


FIG. 4. (a) Site occupation per spin as a function of the on-site energy for different values of doping and $W = 4$, except for the magenta curve with triangles, for which $W = 4.75$. $U = 3$ and $T = 0.01$. (b) Site occupation per spin as a function of the on-site energy for different values of the electronic correlation. $W = 4$, $\delta = 0.4$, and $T = 0.01$.

results for $U = 1$ and $U = 2$, and concluded that the AMI-0 arises for all U , as presented in Fig. 1, arising directly from the metal for small U .

We shall now analyze how the AMI-0 region depends on doping δ and interaction U . As doping increases, carriers are added to the system and more sites become doubly-occupied in comparison with a smaller δ , as can be seen in Fig. 4(a). As a consequence, more disorder has to be added to the system [compare the results for $W = 4.0$ and $W = 4.75$ of the same figure for $\delta = 0.3$] to empty some sites. The AMI-0 thus appears for larger values of disorder when the doping δ increases, as we observe in the phase diagrams of Fig. 1.

We now show in Fig. 4(b) the occupation per site and per spin for $W = 4$, $\delta = 0.4$, and the different values of U . Since single occupation is a characteristic of Mott insulators, the plateau at $\langle n_{i\sigma} \rangle = 0.5$ becomes larger as U increases. For the values of W and δ considered in the figure, the empty sites present for $U = 1$ and $U = 2$ become occupied as we move to $U = 3$. Thus, empty sites “disappear” with either the increase of doping or correlations and, for large U , most of the disorder versus doping phase diagram corresponds to an AMI without empty sites, as we describe in detail in the following section.

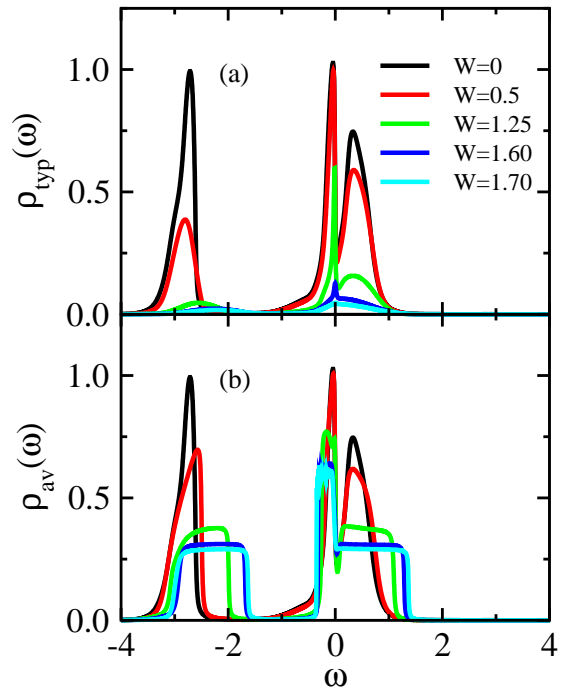


FIG. 5. (a) Typical and (b) average DOS as a function of frequency for different values of disorder W and fixed doping $\delta = 0.2$. $U = 3$ and $T = 0.01$.

IV. AMI PHASE RESULTS FOR $U = 3.0$

We shall now study the AMI without empty sites that appears by increasing interaction U , sandwiched between the AMI-0 and the metallic phase on a large part of the phase diagram. To this purpose, we consider the $U = 3$ case (Fig. 1c), and study the Anderson-Mott transition from the disordered metal by increasing the disorder strength W and various dopings δ . We analyze in particular the behavior of typical and average DOS.

A. Metal-insulator transitions

The DMFT-TMT results for $\rho_{typ}(\omega)$ and $\rho_{av}(\omega)$ are shown, respectively, in panels (a) and (b) of Fig. 5 for fixed $\delta = 0.2$ and different values of disorder W . Since we have small doping, the typical DOS presents a structure of three peaks: two Hubbard bands separated by an energy of the order of U and a quasiparticle-like peak at the Fermi level $\omega = 0$, as it has been previously reported in the clean case.³⁰ According to our results, this holds for small disorder as well, characterizing the system as a correlated metal in this region of parameters.

As disorder W increases, Anderson localization starts to play a role: its effects can be seen by comparing the results for $\rho_{typ}(\omega)$ [panel (a)] and $\rho_{av}(\omega)$ [panel (b)], since the former takes into account only extended states, while the latter includes both extended and localized states of

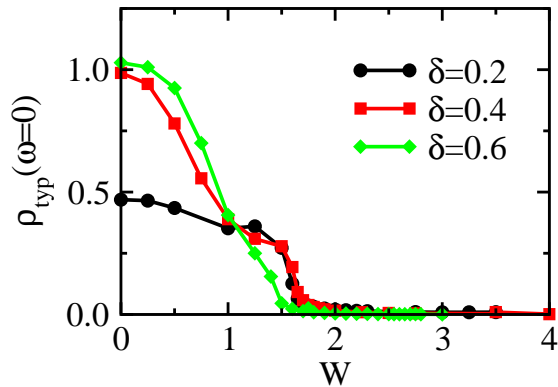


FIG. 6. Typical DOS at the Fermi level as a function of disorder for different values of doping. Results for $\delta = 0.2$ correspond to $\rho_{typ}(\omega)$ shown in panel (a) of Fig. 5. $U = 3$ and $T = 0.01$.

the system. As W increases, states at the band edges localize¹⁵ and we observe that the bands in the typical DOS become smaller. For even more disordered systems, $\rho_{typ}(\omega)$ vanishes on the whole frequency axis, signaling that the system has gone through a disorder-driven MIT. We notice that disorder acts differently on different energy scales. In $\rho_{typ}(\omega)$ Hubbard-like bands around larger values of energy shrink faster than the quasiparticle-like one close to the Fermi level. Notice that $\rho_{av}(\omega)$ remains instead finite at the Anderson-Mott transition. The general effect of disorder appears to be a spreading in energy of the spectral weight, both in the Hubbard bands and at the low-energy quasi-particle peak. This spreading is not symmetrical like at half-filling (see the results in Appendix B), because of the combined effect of disorder and doping.

To determine the critical disorder W_c at which the MIT takes place, it is easier to track the typical DOS at the Fermi level as a function of disorder, as we display in Fig. 6 for different values of doping. This quantity plays the role of an order parameter for the disorder induced MIT, since it is different from zero in the metallic region ($W < W_c$) and is zero in the Anderson-Mott insulator ($W > W_c$). Based on the behavior of $\rho_{typ}(\omega = 0)$ as a function of disorder, we have determined the transition line between the metallic and AMI phases shown in Fig. 1 (red filled dot line). Notice that for $\delta = 0.2$ the maximum of $\rho_{typ}(\omega)$ is close to $\omega = 0$, but not exactly at $\omega = 0$ (in accordance with the results of Ref. 30); this explains why $\rho_{typ}(\omega = 0) \approx 0.5$ for the clean system in Fig. 6, instead of the maximum value of ≈ 1 for $\rho_{typ}(\omega)$ seen in Fig. 5(a).

A key observation is that there exists only a small dependence of W_c with doping δ . As mentioned in Sec. III and observed in Fig. 5(a), the transition to the AMI takes place when all extended states of the system localize. For fixed $U = 3$ (look now at Fig. 2), the range in energy where $\rho_{typ}(\omega)$ extends is roughly doping independent. If doping increases, we observe mainly a transfer of spectral weight from above the Fermi level to energies below it.

This might justify the fact that W_c is practically constant for small to moderate δ . A similar behavior is observed for $U = 1$, but not in the intermediate case of $U = 2$, as we have discussed in Sec. III.

More interesting is the fact that W_c for the doped case is smaller than U , which is the critical disorder at which the transition from the Mott insulator to AMI-0 is seen at half-filling (end of orange line in Fig. 1). This means that the doped Mott insulator is more susceptible to disorder induced localization, as we have already mentioned in Sec. III. By introducing carriers into the system in fact, a narrow band rises within the gap, as seen in our results in Fig. 5(a). By adding disorder to the doped system, this narrow band localizes at a disorder strength which is smaller than the one required to Anderson localize the Mott insulator, which requires that the wide Mott gap is filled due to disorder effects. (For details on how the transition is approached at half-filling see Appendix B.) As mentioned in the previous section, this is not observed for $U = 1$ and $U = 2$, probably because for these values of U the system is in a metallic state at half-filling, and the wide Mott gap is replaced by a wide band of itinerant states around the Fermi level, that can Anderson localize only at higher disorder strengths.

For large doping ($0.75 < \delta < 1.0$), we observe a region within the Anderson-Mott insulator that, with abuse of language, we identify as a band AMI. Starting with the clean system, $\rho_{typ}(\omega)$ shrinks as disorder increases, similar to what happens for small doping. However, for large doping, $\rho_{typ}(\omega = 0)$ becomes zero for a smaller value of disorder (W_c) than that at which the whole band vanishes (W_{c2}). This means that, differently from the low doping case where the whole $\rho_{typ}(\omega)$ vanishes, for $W_c < W < W_{c2}$ the system has still a band of extended states, which is located below the Fermi energy. This behavior is exemplified in Fig. 7 for the case of $\delta = 0.9$: panel (a) shows $\rho_{typ}(\omega)$ for different values of disorder, while panel (b) presents both $\rho_{typ}(\omega = 0)$ and $\zeta = \int_{-\infty}^{\infty} \rho_{typ}(\omega) d\omega$ as a function of W . As we can see, for this value of doping, the system enters into the insulating phase [$\rho_{typ}(\omega = 0) = 0$] at $W_c \approx 1.1$, while all states are localized ($\zeta = 0$) only at $W_{c2} \approx 1.75$. This behavior of $\rho_{typ}(\omega = 0)$ at W_c is reminiscent of that of a band insulator, though the total spectral intensity $\rho_{av}(\omega = 0)$ remains in all cases finite at the Fermi level. Note that W_{c2} approximately coincides with the disorder at which the system enters the AMI region for $\delta < 0.6$, as expected if the vanishing of ζ mainly depends on the U value.

B. Character of the Anderson-Mott insulator

We want now to characterize the physical properties of the AMI region. To this purpose, we shall focus on the (arithmetic) average DOS $\rho_{av}(\omega)$ [defined in eq. (5)], which can be directly connected to spectroscopic experiments. Fig. 8 shows two examples of $\rho_{av}(\omega)$ for $\delta = 0.2$ and $U = 3$: one for which the disorder $W < U$ [panel

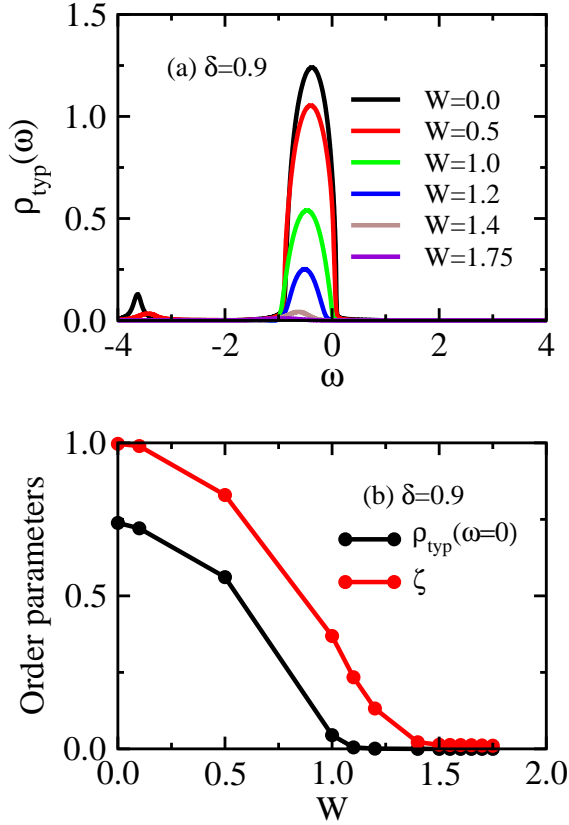


FIG. 7. (a) Typical DOS as a function of energy for different values of disorder W and fixed doping $\delta = 0.9$. (b) Typical DOS at the Fermi level and $\zeta = \int_{-\infty}^{\infty} \rho_{\text{typ}}(\omega) d\omega$ as a function of disorder corresponding to the results in (a). $U = 3$ and $T = 0.01$.

(a)] and another for which $W > U$ [panel (b)]. In both cases the system is in the AMI region, where all states are localized. Since the typical DOS is zero, meaning that there is no bath for the impurities to hybridize, within our TMT approximation impurity sites are effectively in the atomic limit, and the DOS can be calculated with eqs. (5-7) described in Sec. II. In this case, in the absence of disorder ε_i the DOS of a single-impurity problem presents two Dirac delta peaks, one at $\omega = -U/2$ and another at $\omega = U/2$. As disorder ε_i is added, these peaks spread in energy following the flat uniform distribution of the disorder. If disorder is large enough, these rectangles overlap at small frequencies, giving rise to the form of the average DOS seen in Fig. 8.

By looking at the results in panel (a), for $W < U$, we observe that there is a well defined gap at negative energies in $\rho_{\text{av}}(\omega)$. This profile for the DOS reminds us that of the slightly doped Mott insulator. In the case of $W > U$ [panel (b)], on the contrary, a gap is not seen in $\rho_{\text{av}}(\omega)$ anymore. This reminds us of an Anderson insulator. In the insets of the panels, we show the corresponding occupation $\langle n_{i\sigma} \rangle$ per site and per spin as a function of the on-site energy ε_i . In both cases,²⁷ there are sites that are doubly occupied ($\langle n_{i\sigma} \rangle = 1$), as in an

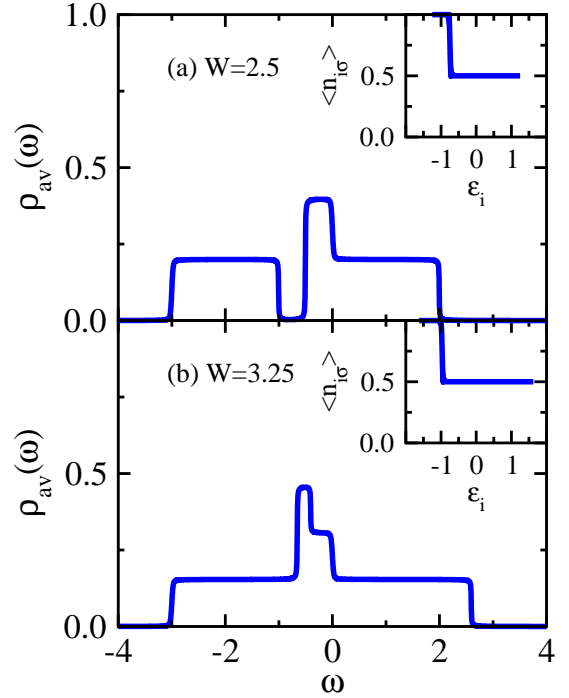


FIG. 8. Average DOS as a function of energy for $U = 3$ and (a) $W = 2.50$ and (b) $W = 3.25$. The insets show the occupation number per site and per spin as a function of the on-site energy for the same parameters of the results in the main panels. $\delta = 0.2$ and $T = 0.01$.

Anderson insulator, and sites that are singly-occupied ($\langle n_{i\sigma} \rangle = 0.5$), as in a Mott insulator (but no empty sites as in the AMI-0 region). Since the two systems have characteristics of Anderson and Mott insulators, we identify both cases as AMI in the phase diagram of Fig. 1. However, we are tempted to say that in the case of panel (a) the role played by Mott mechanism of localization is stronger than that of Anderson effects. Indeed, the correlation U is larger than disorder W and a gap is observed in the average DOS. On the other hand, Anderson mechanism may dominate over the Mott one in the case where disorder is larger than correlations [panel (b)]. In the phase diagram, the first case is observed whenever $W_c < W < U = 3$, while the second corresponds to $W > U = 3$. Similar behavior occurs for $U = 2$ and $\delta > 0.5$, for which there is a region where $W_c < U$.

We recall that at half-filling ($\delta = 0$) the Mott dominated region for $W < W_c \approx U$ presents only singly $\langle n_{i\sigma} \rangle = 0.5$ occupied sites, being double occupation $\langle n_{i\sigma} \rangle = 1$ absent.²⁰ On the other hand, for $W > U$, there exist doubly- and singly-occupied sites, as well as empty ones, and the average DOS has no gap. The presence of this third kind of sites - the empty ones - gives rise to the AMI-0 region, as we described in subsection III A.

In the next subsection, we discuss how the doped system crossovers from the AMI region to the AMI-0 one.

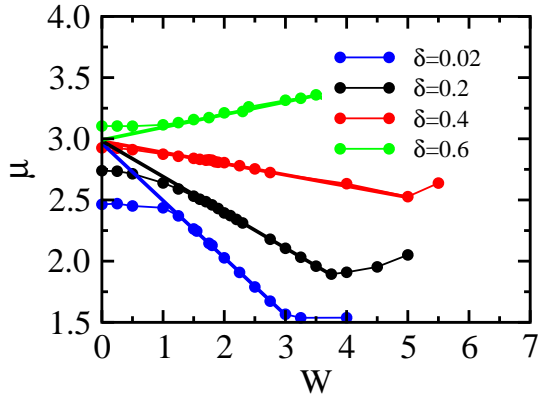


FIG. 9. Chemical potential μ obtained to keep the values of δ fixed as a function of disorder strength. Straight lines correspond to fittings of the numerical results in the range where a linear behavior is observed; note that the lines meet at the point $\mu = U = 3$. $U = 3$ and $T = 0.01$.

C. Crossover to the AMI-0 region

Finally, it is useful to see the behavior of the chemical potential μ as a function of disorder for fixed doping, showed in Fig. 9, again for $U = 3$. In the metallic phase (for small values of W), the μ vs. W curve is markedly horizontal. By entering into the AMI, above $W \approx 1.75$, the μ vs. W follows closely a linear law $\mu = (\delta - 0.5)W + U$. By further increasing disorder, the μ vs. W curve displays once again a sharp change in slope when entering into the AMI-0 that presents empty sites. For δ values in this AMI-0 region, μ always increases with W .

The linear μ vs. W behavior in the AMI region allows us to establish an equation determining the disorder dependence of the line separating the AMI-0 and AMI regions. We profit again that within the DMFT-TMT method in the AMI region each impurity site is in the atomic limit (as described in Sec. II). In this case, the site is empty if its on-site energy $\varepsilon_d = \varepsilon_i - \mu > 0$ (eq. 6). The value of the disorder where the first empty site forms must coincide with the highest possible value of on-site energy $\varepsilon_i = W/2$, i.e. $W/2 = \mu$. Plugging this value of μ into the μ vs. W linear relation, which holds up to the crossover to the AMI-0 region, we obtain:

$$W = \frac{U}{1 - \delta}. \quad (8)$$

Equation 8, which we display in Fig. 1 as a dashed gray line, well describes the crossover between AMI and AMI-0 regions that we establish numerically (brown diamond symbols in the figure).

V. CONCLUSION

In this work, we solved the Anderson-Hubbard model in the doped case by using the combination of Dynamical Mean Field Theory and Typical Medium Theory.

The former describes the Mott transition, while the latter takes into account Anderson localization effects. We built the disorder versus doping phase diagram for three values of U : $U = 1$, $U = 2$, and $U = 3$, in units of the clean, non-interacting bandwidth. For any interaction, there is a region of the phase diagram where we observe an Anderson-Mott insulator similar to the one that exists at half-filling, with the presence of empty sites in the system (AMI-0). As doping (and thus the number of carriers in the system) increases, the empty sites that exist at small doping become occupied, giving rise to a different Anderson-Mott insulator (AMI). When the electronic interaction becomes stronger, the AMI wedges between the metallic phase and the AMI-0, occupying large part of the phase diagram in the strongly correlated regime, for $U = 3$. This is a consequence of the fact that the disorder-driven MIT takes place for a much smaller disorder strength in the doped, strongly correlated regime than in the weakly correlated regime or at half-filling. An intermediate behavior should appear in the intermediate correlated regime, with the critical disorder W_c monotonically decreasing with doping, as portrayed in the phase diagram (Fig. 1) for $U = 2$.

Upon doping, the properties of the system are therefore strongly determined by the combined effect of disorder, interaction, and doping to form an insulator presenting at the same time Anderson and Mott-Hubbard features. The evolution of the phase diagram as a function of disorder and doping, that we presented in this work from the weak to strongly correlated regime, should determine the universal properties of the disorder-driven MIT.

ACKNOWLEDGMENTS

We acknowledge Eduardo Miranda and Marcelo Rozenberg for discussions and Jakska Vučićević and Darko Tanasković for the development of the IPT single-impurity code used in our calculations. This work is supported by FAPEMIG, CNPq (in particular through INCT-IQ 465469/2014-0), and CAPES (in particular through programs CAPES-COFECUB-0899/2018 and CAPES-PrInt-UFGM (M.C.O.A.)). M.C. acknowledges support from the ANR grant NEPTUN no. ANR-19-CE30-0019-04.

Appendix A: Spectra and metal-insulator transition at strong $U > 3$

We shall show here that the results on the MIT that we established for the $U = 3$ case are qualitatively similar for larger interaction U . Interaction has the effect of changing the position of the DOS bands. In the presence of doping, only the low energy band moves proportionally to the U value. A quasiparticle-like band remains around the Fermi level; its position does not change by increasing U to keep the doping δ fixed. In Fig. 10(a), where we

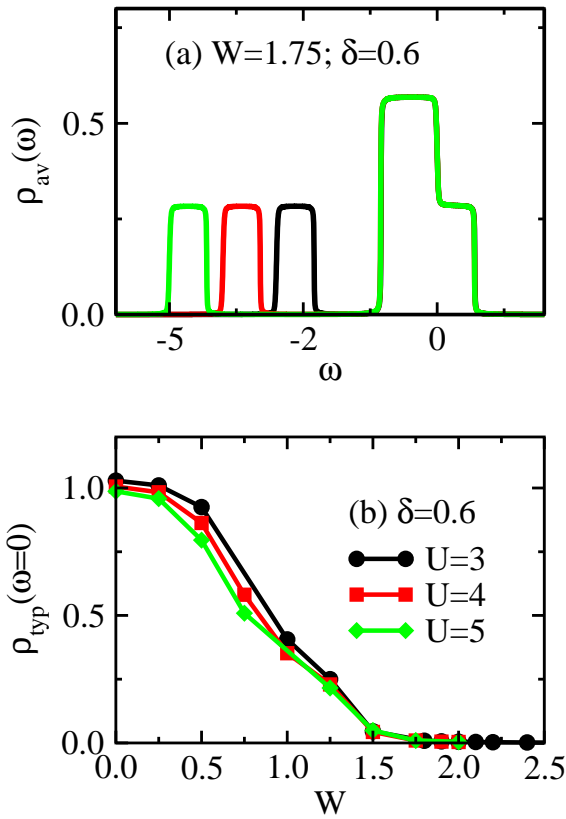


FIG. 10. Results for large values of the interaction, $U = 3$, $U = 4$, and $U = 5$. (a) Average DOS as a function of frequency when $W = 1.75$. (b) Typical DOS at the Fermi level as a function of W , showing that the order parameter goes to zero for the same value of W_c (for $U \geq 3$). $\delta = 0.6$ and $T = 0.01$.

display the average DOS $\rho_{av}(\omega)$, we can see an example of this behavior: increasing the interaction does not change the Fermi level. This causes the value of W_c not to change, as can be seen in Fig. 10(b). This phenomenon only occurs when the bands are far apart (in the Mott regime $W < U$ of the doped AHM).

Appendix B: Results for $U = 3$ at half-filling

The evolution of the typical and average DOS as disorder increases for the case of $U = 3$ and no doping is presented in Fig. 11. The clean system has a Mott gap, which starts to be filled with localized states as disorder increases. The gap eventually closes and the system becomes an Anderson-Mott insulator, as illustrated in Fig. 11 for $W = 3.5$. At half-filling, the Anderson-Mott insulator always presents empty sites and thus corresponds to the AMI-0 defined in the main text. This behavior is different than the one presented in Fig. 5 for the doped case, where the clean system is a metal.

-
- ¹ N. F. Mott, *Metal-insulator transitions* (Taylor and Francis, 1974).
 - ² J. Hubbard, Proceedings of the Royal Society of London. Series A. Mathematical and Physical Sciences **281**, 401 (1964).
 - ³ M. Imada, A. Fujimori, and Y. Tokura, Rev. Mod. Phys. **70**, 1039 (1998).
 - ⁴ E. Dagotto, Science **309**, 257 (2005).
 - ⁵ D. McWhan, A. Menth, J. Remeika, W. F. Brinkman, and T. Rice, Phys. Rev. B **7**, 1920 (1973).
 - ⁶ P. Limelette, A. Georges, D. Jérôme, P. Wzietek, P. Metcalf, and J. Honig, Science **302**, 89 (2003).
 - ⁷ P. W. Anderson, Phys. Rev. **109**, 1492 (1958).
 - ⁸ P. A. Lee and T. Ramakrishnan, Rev. Mod. Phys. **57**, 287 (1985).
 - ⁹ E. Miranda and V. Dobrosavljević, Reports on Progress in Physics **68**, 2337 (2005).
 - ¹⁰ E. Abrahams, S. V. Kravchenko, and M. P. Sarachik, Rev. Mod. Phys. **73**, 251 (2001).
 - ¹¹ S. V. Kravchenko and M. P. Sarachik, in *50 Years of Anderson Localization*, edited by E. Abrahams (World Scientific, Singapore, 2010) Chap. 17, pp. 361–384.
 - ¹² E. Lahoud, O. N. Meetei, K. B. Chaska, A. Kanigel, and N. Trivedi, Phys. Rev. Lett. **112**, 206402 (2014).
 - ¹³ Z. Wang, Y. Okada, J. O’Neal, W. Zhou, D. Walkup, C. Dhital, T. Hogan, P. Clancy, Y.-J. Kim, Y. Hu, *et al.*, Proceedings of the National Academy of Sciences **115**, 11198 (2018).
 - ¹⁴ A. Georges, G. Kotliar, W. Krauth, and M. J. Rozenberg, Rev. Mod. Phys. **68**, 13 (1996).
 - ¹⁵ J. M. Ziman, *Models of disorder* (Cambridge University Press, 1979).
 - ¹⁶ V. Dobrosavljević, A. A. Pastor, and B. K. Nikolić, Europhys. Lett. **62**, 76 (2003).
 - ¹⁷ S. Mahmoudian, S. Tang, and V. Dobrosavljević, Phys. Rev. B **92**, 144202 (2015).
 - ¹⁸ A. Ostlin, Y. Zhang, H. Terletska, F. Beiușeanu, V. Popescu, K. Byczuk, L. Vitos, M. Jarrell, D. Vollhardt, and L. Chioncel, Phys. Rev. B **101**, 014210 (2020).
 - ¹⁹ K. Byczuk, W. Hofstetter, and D. Vollhardt, Phys. Rev. Lett. **94**, 056404 (2005).
 - ²⁰ M. C. O. Aguiar, V. Dobrosavljević, E. Abrahams, and G. Kotliar, Phys. Rev. Lett. **102**, 156402 (2009).
 - ²¹ K. Byczuk, W. Hofstetter, and D. Vollhardt, Phys. Rev. Lett. **102**, 146403 (2009).

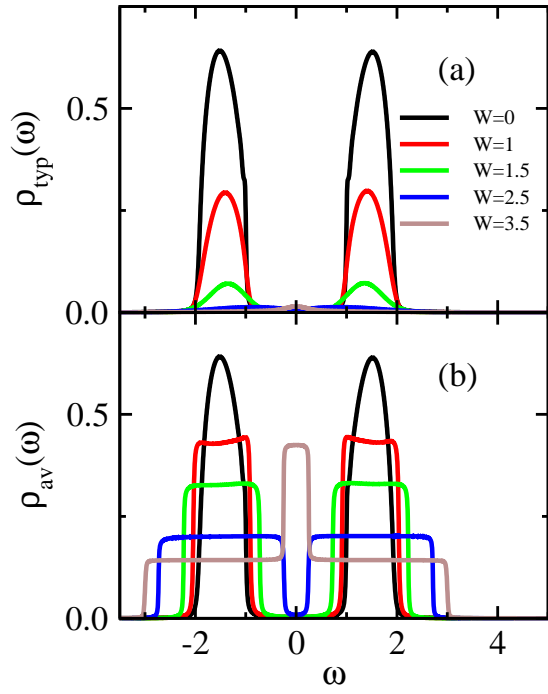


FIG. 11. (a) Typical and (b) average DOS as a function of energy for different values of disorder W at half-filling. $U = 3$ and $T = 0.01$.

- ²² H. Bragança, M. C. O. Aguiar, J. Vučićević, D. Tanasković, and V. Dobrosavljević, Phys. Rev. B **92**, 125143 (2015).
- ²³ J. Skolimowski, D. Vollhardt, and K. Byczuk, Phys. Rev. B **92**, 094202 (2015).
- ²⁴ C. E. Ekuma, S.-X. Yang, H. Terletska, K.-M. Tam, N. S. Vidhyadhiraja, J. Moreno, and M. Jarrell, Phys. Rev. B **92**, 201114(R) (2015).
- ²⁵ S. Sen, H. Terletska, J. Moreno, N. S. Vidhyadhiraja, and M. Jarrell, Physical Review B **94**, 235104 (2016).
- ²⁶ S. Sen, N. S. Vidhyadhiraja, and M. Jarrell, Phys. Rev. B **98**, 075112 (2018).
- ²⁷ M. C. O. Aguiar, V. Dobrosavljević, E. Abrahams, and G. Kotliar, Phys. Rev. B **73**, 115117 (2006).
- ²⁸ D. B. McWhan, T. M. Rice, and J. P. Remeika, Phys. Rev. Lett. **23**, 1384 (1969).
- ²⁹ D. B. McWhan, J. P. Remeika, T. M. Rice, W. F. Brinkman, J. P. Maita, and A. Menth, Phys. Rev. Lett. **27**, 941 (1971).
- ³⁰ H. Kajueter and G. Kotliar, Phys. Rev. Lett. **77**, 131 (1996).
- ³¹ M. Potthoff, T. Wegner, and W. Nolting, Phys. Rev. B **55**, 16132 (1997).
- ³² T. Wegner, M. Potthoff, and W. Nolting, Phys. Rev. B **57**, 6211 (1998).
- ³³ A. Hewson, *The Kondo Problem to Heavy Fermions* (Cambridge University Press, 1997).